Knockout of zebrafish desmin genes does not cause skeletal muscle degeneration but alters calcium flux

Gulsum Kayman Kurekci[1], Ecem Kural Mangit[1,2], Cansu Koyunlar[1,3], Seyda Unsal[1,4], Berk Saglam[5], Bora Ergin[5], Merve Gizer[6], Ismail Uyanik[7], Niloufar Boustanabadimaralan Düz[1], Petek Korkusuz[8], Beril Talim[9], Nuhan Purali[4], Simon M. Hughes[10], Pervin R. Dincer[1]*.

[1]Department of Medical Biology, Hacettepe University Faculty of Medicine, Ankara, 06100, Turkey

[2]Laboratory Animals Research and Application Centre, Hacettepe University, Ankara, 06100, Turkey

[3]Current address: Department of Hematology, Erasmus MC, Rotterdam, 3015 CN, The Netherlands

[4]Current address: Department of Cancer and Inflammation, The Institute of Molecular Medicine, University of Southern Denmark, Odense C, 5000, Denmark

[5]Department of Biophysics, Hacettepe University Faculty of Medicine, Ankara, 06100, Turkey.

[6]Department of Stem Cell Sciences, Hacettepe University Graduate School of Health Sciences, Ankara, 06100, Turkey

[7]Department of Electrical and Electronics Engineering, Hacettepe University Faculty of Engineering, Ankara, 06800, Turkey

[8]Histology and Embryology, Hacettepe University Faculty of Medicine, Ankara, 06100, Turkey

[9]Department of Pediatrics, Pathology Unit, Hacettepe University Faculty of Medicine, Ankara, 06100, Turkey

[10]Randall Centre for Cell and Molecular Biophysics, New Hunt's House, Guy's Campus, King's College London, London, SE1 1UL, United Kingdom

*Correspondence to pdincer@hacettepe.edu.tr

Abstract

Desmin is a muscle-specific intermediate filament protein that has fundamental role in muscle structure and force transmission. Whereas human desmin protein is encoded by a single gene, two desmin paralogs (*desma* and *desmb*) exist in zebrafish. *Desma* and *desmb* show differential

spatiotemporal expression during zebrafish embryonic and larval development, being similarly expressed in skeletal muscle until hatching, after which expression of *desmb* shifts to gut smooth muscle. We generated knockout (KO) mutant lines carrying loss-of-function mutations for each gene by using CRISPR/Cas9. Mutants are viable and fertile, and lack obvious skeletal muscle, heart or intestinal defects. In contrast to morphants, knockout of each gene did not cause any overt muscular phenotype, but did alter calcium flux in myofibres. These results point to a possible compensation mechanism in these mutant lines generated by targeting nonsense mutations to the first coding exon.

Introduction

Desmin is a type III intermediate filament protein that is specifically expressed in skeletal, cardiac and smooth muscles. In addition to their fundamental role in maintaining the structural integrity of the sarcomere, desmin intermediate filaments are involved in mechanotransduction and organelle positioning. Desminopathies belonging to myofibrillar myopathies are primarily characterized by abnormal protein aggregates in muscle and present as progressive skeletal myopathy and/or cardiomyopathy[1]. Although the involvement of smooth muscles is not widely reported, some patients suffer from smooth muscle dysfunction such as swallowing difficulties, intestinal pseudo-obstruction and respiratory insufficiency[2–4]. The majority of desmin mutations are associated with desmin aggregates; however, some mutations have been reported to not alter filament assembly and network integrity *in vivo* or *in vitro*[5,6]. KO of desmin in mice does not affect the viability and the development of muscles; however, muscle degeneration and cardiomyopathy are observed[7,8].

Zebrafish is a widely used model for neuromuscular disorders[9,10]. Besides the advantage of being the most abundant tissue in zebrafish; the gene profile, and the structural and histological features of mammalian skeletal muscle are highly preserved in zebrafish[11]. To date, two approaches have been used to study the effect of the loss of desmin in zebrafish. On one hand, it was shown that morpholino-mediated knockdown of desmin causes skeletal and cardiac muscle myopathy[12,13]. On the other hand, Ramspacher et al. studied a desmin mutant line (*desma*^{sa5}), generated by ENU mutagenesis, which causes a truncation mutation approximately half way along the molecule, that also presented with skeletal and cardiac muscle phenotype[14].

Gene duplications are common in zebrafish and most duplicated genes have similar functions to their human orthologs. Alternatively, paralogs can be expressed in different tissues or stages of development and have distinct functions to their human orthologs. Humans carry a single copy of the *DES* gene whereas two desmin genes (*desma* and *desmb*) are found in zebrafish[13]. Previous work has not established the tissue specific distribution and role of these two desmin paralogs.

Here, we report the spatiotemporal expression pattern of the two desmin paralogs in zebrafish, as well as the generation using CRISPR/Cas9 and characterization of putative null zebrafish mutant lines for each of the desmin paralogs. We show that *desma* and *desmb* are expressed in skeletal muscle until 72-hour post-fertilization (hpf). After 72 hpf, expression of *desmb* shifts to gut smooth muscle. Putative null mutation of each gene does not affect viability and adults do not develop any overt phenotype. However, altered calcium flux was observed in *desma*-KO myofibres. These results show that loss-of-function of desmin genes by mutations in the first coding exon result in a mild phenotype with no visible muscle degeneration but altered calcium flux, in contrast to morpholino-mediated knockdown models and the $desma^{sa5}$ allele.

RESULTS

Zebrafish desmin genes

In contrast to the single mammalian *DES* gene, zebrafish have two desmin orthologs, *desma* (*desmin a*) and *desmb (desmin b)*, which are paralog genes located on chromosome 9 and 6, respectively. Zebrafish *desma* and *desmb* paralogs share 81% and 83% identity with human *DES* gene. Although a single transcript is known to be encoded by human *DES* gene, in ENSEMBL two isoforms are predicted to be transcribed from zebrafish *desma*; *desma-1* mRNA coding for a 488 amino acid protein (predicted molecular weight of 55.7 kDa) and *desma-2* mRNA coding for a 473 amino acid protein (predicted molecular weight of 54.1 kDa). In *desma-2* transcript, exon 9 is skipped, corresponding to 15 amino acids located in the tail domain of Desma-1 protein (Supplementary Fig. S1 online). The 473 amino acid Desmb protein is predicted to have a molecular weight of 54.2 kDa. At the amino acid level, zebrafish Desma-1, Desma-2 and Desmb show 80%, 82% and 83% similarity with human desmin protein.

87 **Differential expression of desmin transcripts during zebrafish development**

88 We analyzed the spatiotemporal expression patterns of *desma* and *desmb* genes during zebrafish
89 development at several stages beginning from somitogenesis until 5 days post fertilization (dpf)
90 by whole mount *in situ* hybridization (ISH). For detecting both *desma* transcripts (*desma-2* lacks
91 exon 9), we synthesized an antisense probe by using a forward primer binding to exon 1 and a
92 reverse primer binding to exon 10 (Supplementary Fig. S1 online). No specific staining was
93 observed in embryos treated with sense probes for each gene (Supplementary Fig. S2 online).
94 *Desma* was first detected at 11 hpf in adaxial slow muscle precursor cells when the first somites
95 form and remained strongly expressed in somites at all examined stages (Fig. 1a). *Desma* was also
96 expressed in the developing heart from 35 hpf (Fig. 1b). Cryosections of 72 hpf embryos showed
97 that *desma* was distributed in the entire somite, including epaxial and hypaxial muscles (Fig. 1c).
98 By 72 hpf, *desma* was expressed in cranial muscles including external ocular muscles, opercular
99 muscles and mandibular muscles (Fig. 1d). At 96 hpf, transversal sections revealed *desma*
100 expression at the anterior intestine (Fig. 1d, upper panel). At 72, 96 and 120 hpf, expression of
101 *desma* in pectoral fin muscles was clearly visible (Fig. 1d). *Desmb* had an overlapping expression
102 pattern to *desma* from the beginning of somitogenesis until 72 hpf, including staining in trunk
103 somites and heart (Fig. 1a, b). At 72 hpf, somitic expression of *desmb* dramatically decreased with
104 a residual expression in the lateral edges of the myotome. By contrast, strong signal of *desmb*
105 transcripts was detected around the gut throughout the length of the intestine (Fig. 1a, c, e). Similar
106 to *desma*, *desmb* was also expressed in pectoral fin muscles, operculum muscles and mandibular
107 muscles at 72 hpf (Fig. 1e). These results indicate that *desma* and *desmb* expression partially
108 overlap during zebrafish muscle development. As the gut develops, *desmb* expression shifts from
109 somitic muscle to intestinal smooth muscle.

110 **Generation of *desma* and *desmb* knockout zebrafish lines**

111 *Desma* and *desmb* mutant zebrafish lines were generated by using CRISPR/Cas9 genome editing.
112 The $desma^{kg97}$ line exhibited 2 bp deletion and 4 bp insertion in the first exon
113 (g.198_99delGAinsTGAT, NC_007120.7) leading to a frameshift at amino acid 45 and a
114 premature stop codon after four amino acids. In the $desmb^{kg156}$ mutant line, a 5 bp deletion in exon
115 1 (c.245_249delCTTAT, NM_001077452.1) resulted in a frameshift at amino acid 82 and
116 introduced a premature stop codon after three amino acids (Fig. 2a). Heterozygous mutants showed

117 no defect and homozygous mutant embryos and larvae developed relatively normally, at least for
118 the first few days (Fig. 2d).

119 **Expression of *desma* and *desmb* in knockout lines**

120 Mutations were predicted to trigger nonsense-mediated decay of mRNA or synthesis of short
121 truncated polypeptides. As expected, qRT-PCR revealed a significant decrease of *desma*
122 transcripts in *desma*^{kg97} homozygous embryos (P=0.0286, Mann-Whitney U), while *desmb*
123 transcripts were significantly decreased in *desmb*^{kg156} homozygous embryos at 96 hpf compared to
124 wild type (WT) (P=0.0286, Mann-Whitney U) (Fig. 2b). Consistent with El-Brolosy et al.[15], weak
125 *desmb* or *desma* mRNA up-regulation may occur in the respective mutant embryos (Fig. 2b).

126 In order to investigate the potential compensatory effect of *desmin* paralog upregulation in
127 mutant embryos, expression patterns of *desmb* and *desma* transcripts were determined in *desma*^{kg97}
128 or *desmb*^{kg156} homozygous mutant embryos, respectively. In *desma*$^{kg97/kg97}$ embryos, the expression
129 pattern of *desmb* transcripts (Fig. 2c) was similar to that of wild-type embryos (Fig. 1a). Somitic
130 expression of *desmb* was observed in *desma*$^{kg97/kg97}$ at 48 hpf, and a shift towards gut expression
131 after 72 hpf. Beyond 72 hpf, no *desmb* staining was detected in somites of *desma*$^{kg97/kg97}$ embryos.
132 In *desmb*$^{kg156/kg156}$ embryos, *desma* was still strongly expressed in somites and visible in the
133 anterior intestine at 96 hpf (Fig. 2c). In order to confirm the loss-of-function of desmin in mutants
134 at the protein level, expression of Desma and Desmb in WT, *desma*^{kg97} or *desmb*^{kg156} homozygous
135 embryos at 96 hpf was determined by immunofluorescence staining using a desmin antibody
136 recognizing both Desma and Desmb (Fig. 3). In WT embryos, desmin staining was detected in
137 both somites and gut. As expected from ISH results, somitic expression was lost and gut was
138 preferentially stained in *desma*$^{kg97/kg97}$ mutants. In *desmb*$^{kg156/kg156}$ mutants, expression in somites
139 and anterior intestine were preserved while staining of the middle and posterior intestine was lost.
140 We conclude that mutation of each gene reduces the cognate mRNA and protein at all stages
141 examined and that compensation by up-regulation of the unmutated paralogous gene is at best very
142 weak.

143 **General larval characteristics of desmin mutants**

144 In order to evaluate the effects of the absence of *desma* or *desmb* on development, WT, *desma*^{kg97}
145 and *desmb*^{kg156} homozygous embryos/larvae were compared. No significant difference was

146 observed in the number of viable eggs between *desma*$^{kg97/kg97}$ and WT (*P*=0.6842, Mann-Whitney
147 U) or *desmb*$^{kg156/kg156}$ and WT (*P*=0.9654, Mann-Whitney U) (Fig. 4a). Hatching period (48-72
148 hpf[16]) is a critical process in embryonic development and reduction in the hatching rate could be
149 associated with reduced muscle function[17]. The time course showed that although different
150 hatching times were observed between groups, no significant difference was found between
151 hatching rates of mutant and WT embryos at 72 hpf with over 94% of embryos hatched
152 (*desma*$^{kg97/kg97}$ vs. WT, *P*=0.9902; *desmb*$^{kg156/kg156}$ vs WT, *P*=0.3186, repeated measures two-way
153 ANOVA, Bonferroni post *hoc* test) (Fig. 4b).
154 Similar mortality rates were observed with no significant difference between homozygous
155 mutants of *desma*^{kg97} or *desmb*^{kg156} and WT embryos (*desma*$^{kg97/kg97}$ vs. WT, *P*=0.1287;
156 *desmb*$^{kg156/kg156}$ vs. WT, *P*=0.6239, repeated measures two-way ANOVA) (Fig. 4d). Finally,
157 among surviving larvae, no statistically significant difference in body length was observed
158 between WT and mutant groups (*P*=0.2036 for WT vs. *desma*$^{kg97/kg97}$; *P*=0.1893 for WT vs.
159 *desmb*$^{kg156/kg156}$, Mann-Whitney U) (Fig. 4c).

160 **Mutant larvae show no neuromuscular defect**

161 Muscle fibre integrity and somite morphology length were investigated by staining muscle actin
162 with rhodamine phalloidin in 96 hpf embryos (Fig. 4e). At this stage, mainly *desma* is expressed
163 in somites. No muscle lesion or detachment of fibres was observed in mutants and no significant
164 difference was found in somite length, fibre diameter and nuclei number between mutants and WT
165 (Supplementary Fig. S3 online).
166 Touch-evoked response assay is a widely used method to assess neuromuscular function
167 in 48 hpf zebrafish embryos[18]. We performed motility experiments in a blinded manner on siblings
168 from three groups of heterozygous mutant in-crosses and genotyped them after. First, the average
169 escape time of siblings from *desma*$^{kg97/+}$ in-crosses was assessed and no significant difference was
170 found in *desma*^{kg97} heterozygous (*P*=0.122, Mann-Whitney U) or homozygous (*P*=0.5529, Mann-
171 Whitney U) mutants compared to WT (Fig. 4f). Similarly, no significant difference in the average
172 escape time was found in *desmb*^{kg156} heterozygous (*P*=0.3968, Mann-Whitney U) or homozygous
173 (*P*=0.6131, Mann-Whitney U) mutants compared to WT (Fig. 4g). Since both *desma* and *desmb*
174 are expressed in somites up to this stage (48 hpf) and might potentially compensate for the absence
175 of each other, we finally evaluated the effect of the absence of both proteins in siblings from

176 *desma*$^{kg97/+}$;*desmb*$^{kg156/kg156}$ double mutants. No significant difference in the average escape time
177 was found in homozygous double mutants (*desma*$^{kg97/kg97}$;*desmb*$^{kg156/kg156}$) compared to
178 *desma*$^{+/+}$;*desmb*$^{kg156/kg156}$ (P=0.3165, Mann-Whitney U) and in *desma*$^{kg97/+}$;*desmb*$^{kg156/kg156}$
179 embryos compared to *desma*$^{+/+}$;*desmb*$^{kg156/kg156}$ (P = 0.2334, Mann-Whitney U) (Fig. 4h).

180 **Mutant adult skeletal muscle shows no muscle degeneration**

181 Because no skeletal muscle phenotype was observed in mutant larvae, surviving one-year-old
182 adults were investigated for muscle defects. Some homozygous single and double mutants
183 survived until adulthood with no sign of behavioral defect (Fig. 5a). Western blot was performed
184 using myotomal skeletal muscle protein extracts isolated from adult fish (WT, homozygous and
185 heterozygous *desma*^{kg97} mutants, homozygous and heterozygous *desmb*^{kg156} mutants and
186 *desma*$^{kg97/kg97}$;*desmb*$^{kg156/kg156}$ double mutants). As *desma* was shown to be predominantly
187 expressed in somites from 72 to 120 hpf, the two bands detected in WT and *desmb*^{kg156} mutants
188 were predicted to correspond to Desma-1 (predicted molecular weight 55.7 kDa) and Desma-2
189 (predicted molecular weight 54.1 kDa) isoforms. In agreement with that, both bands were absent
190 in *desma*^{kg97} homozygous mutant and double mutants while still expressed in homozygous
191 *desmb*^{kg156} mutant (Fig. 5b). No *desmb* mRNA upregulation was observed in *desma*$^{kg97/kg97}$ adult
192 skeletal muscle, nor significant *desma* mRNA upregulation in *desmb*$^{kg156/kg156}$ compared to WT.
193 Moreover, *desmb* mRNA expression was >1200-fold lower than *desma* in WT adult skeletal
194 muscle tissue, confirming that Desma is the predominantly expressed paralog in adult skeletal
195 muscle tissue (Supplementary Fig. S4 online).

196 Histopathological examination of hematoxylin-eosin stained skeletal muscle tissue
197 sections revealed no pathological changes in homozygous single mutants compared to WT (Fig.
198 5c). General morphology of skeletal muscle fibre shape and size, integrity of sarcoplasm and
199 interstitium were normal. Mild variation in fibre size was present in both WT and mutant fish.
200 Signs of degeneration or regeneration, internal nuclei, inflammatory cell infiltration and increase
201 in connective or adipose tissue in interstitium were absent (Fig. 5c).

202 Transmission electron microscopy revealed intact sarcolemma, generally peripherally,
203 unfrequently centrally located healthy euchromatic nuclei with well determined nucleoli and
204 perinuclear cisternae in adult WT, *desma*$^{kg97/kg97}$ and *desmb*$^{kg156/kg156}$ skeletal muscle tissue samples
205 (Fig. 6a-f). WT and both mutant samples presented pleomorphic mitochondria with well-defined

206 tubular cristae. Mitochondria making rows or clusters and exhibiting fission and mitophagy were
207 common in all groups (Fig. 6g-l). The sarcoplasmic reticulum and T-tubule system-associated
208 triads appeared locally proliferated and enlarged in all samples (Fig. 6p-r). These membrane
209 systems caused the shift of the sarcomeric organization to some extent in both WT and mutant
210 samples (Fig. 6a-c, m-r). Ultrastructural evaluation revealed a similar myofilament organization
211 in all group's muscle samples. The Z lines were generally aligned in most of the fibres in all groups
212 (Fig. 6a-c). A limited number of Z line streaming or duplication was noted in both WT and
213 knockout muscle specimens (Fig. 6m-o). As expected, no deposit or particle was noted in any of
214 the groups. We conclude that fish entirely lacking wild-type Desma generate and maintain
215 functional skeletal muscle in the context of a zebrafish aquarium.

216 **Altered calcium flux in *desma* mutant fibres**

217 Although anatomically apparently wild-type, adult *desma*$^{kg97/kg97}$ mutants were physiologically
218 defective in calcium handling. To investigate amplitude and time course of calcium signals
219 released in response to a depolarizing voltage stimulus, individual fibres were dissected from WT
220 (N=8), *desma*^{kg97} (N=11) or *desmb*^{kg156} (N=8) homozygous mutant 1-year-old fish. Calcium flux
221 along fibres was monitored in the isolated fibres by Fluo-4 AM after four consecutive depolarizing
222 stimuli with the amplitude of the current pulse kept constant at 100 nA and the duration increased
223 by 10 ms at each pulse (Fig. 7a-b). Amplitudes of the calcium emission signals in the first (10 ms)
224 stimulus and fourth (40 ms) stimulus were compared between mutants and WT. To eliminate
225 variance induced by amplitude, offset and fibre size differences, amplitude values were baseline
226 corrected and divided by the diameter of each fibre. Amplitudes of the first and the fourth calcium
227 transient were significantly lower in *desma*$^{kg97/kg97}$ fibres compared to WT fibres (P=0.0008 for
228 first transient; P=0.0025 for fourth transient, Mann-Whitney U) (Fig. 7c-d). In contrast, no
229 significant difference was found in the amplitude of calcium flux between *desmb*$^{kg156/kg156}$ fibres
230 and WT fibres (P=0.0881 for first transient; P=0.6657 for fourth transient, Mann-Whitney U) (Fig.
231 7c-d).

232 Time course of the longest calcium transient (40 ms, fourth transient) has been analyzed
233 for comparing the waveform of the responses and dissecting the phases of the transient. Signals
234 have been baseline corrected and then normalized. Mean amplitude values as a function of time
235 were compared between *desma*$^{kg97/kg97}$ and WT or *desmb*$^{kg156/kg156}$ and WT. No significant

236 difference was found in the rising and the plateau phases of the recorded transients between the
237 experimental groups (Figure 7e). However, the decay phase was significantly faster in
238 *desma*$^{kg97/kg97}$ mutant fibres compared to WT (* indicates $P<0.05$, repeated measures ANOVA,
239 Bonferroni post *hoc* test). No significant difference was found in *desmb*$^{kg156/kg156}$ mutant fibres
240 compared to WT (Fig. 7e).

241 DISCUSSION

242 Although previous studies showed that *desma* is the main gene expressed in somites, no study did
243 clearly distinguish spatial and temporal differences in the expression of the two genes. We showed
244 that until 72 hpf *desma* and *desmb* expressions overlap in somites and heart but later in
245 development, *desmb* expression shifts from somites to intestinal smooth muscle, and *desma*
246 remains as the predominantly expressed paralog in adult somites. Note that the residual *desmb*
247 expression detected in the lateral edges of the myotome might reflect a transient expression in new
248 skeletal muscle fibres (Fig. 1c)[19]. *In silico* prediction of transcription factor (TF) binding sites on
249 *desma* and *desmb* putative promoters revealed 14 and 7 muscle-related TFs unique to *desma* and
250 *desmb,* respectively (Supplementary Table S2 online). TFs exclusively binding to *desma* promoter
251 were enriched in striated muscle (12 out of 14 TFs) while TFs unique to *desmb* promoter were
252 enriched in smooth muscle (5 out of 7 TFs). This preliminary data supports the hypothesis that
253 *desma* and *desmb* expressions are differentially regulated throughout zebrafish muscle
254 development and experimental confirmation would bring further insight into their transcriptional
255 regulation. Lack of desmin in mice affects multiple tissues including myocardium, skeletal muscle,
256 intestinal smooth muscle and smooth muscle of the aorta[8]. Since Desmb appears to be the major
257 Desmin in smooth muscle in zebrafish, at least in the gut, zebrafish *desmb* mutants may be
258 particularly useful for understanding the role of desmin in smooth muscle without interference by
259 additional phenotypes from skeletal muscle. It should be noted that vascular defects have been
260 observed in *desma*^{sa5} mutant hearts where *desmb* expression is not affected; therefore, it would be
261 interesting to investigate the expression of *desma* in early smooth muscle development and
262 endothelial cells. Also, comparison of the filament-forming capacity of Desma and Desmb would
263 offer further insight into their functional redundancy. Although not the focus of this study, it should
264 be noted that heart and gastrointestinal development in mutant lines have not been extensively

265 analyzed; however; no heart oedema such as observed in desmin morphant or overt morphological
266 abnormality in the gut have been observed in *desma*^{kg97} or *desmb*^{kg156} embryos and adults.

267 Reduced *desma* or *desmb* mRNAs in their respective mutants suggest the mRNAs are
268 degraded by nonsense-mediated decay, such that only tiny amounts of the severely truncated
269 proteins would be produced. Such fragments lack the highly conserved α-helical central rod
270 domain responsible for filament formation and all known protein-protein interaction domains of
271 Desmin[20]. Intriguingly, no overt skeletal muscle phenotype was observed in desmin knockout
272 mutants. These results are in contrast to those reported for desmin morphants where both *desma*
273 and *desmb* were targeted with morpholinos[13] and for ENU-induced *desma*^{sa} knockout mutants[21].
274 Both morphants and mutants embryos exhibited disorganized fibres, disrupted sarcomeres and
275 altered motility. Our findings raise the possibility that a haploinsufficient dominant effect in
276 *desma*^{sa5} mutants may disrupt muscle; such an explanation would no account for the morphant
277 phenotype. We conclude that at least two further alleles of *desma* may be needed to resolve these
278 differences: firstly, a full locus or promoter deletion allele that would simultaneously prevent any
279 Desmin polypeptide synthesis and any RNA-triggered compensation and, secondly, an allele
280 lacking morpholino binding ability but nevertheless encoding wild-type protein to prove that the
281 morphant phenotype is due to *desma* binding.

282 Many loss-of-function mutants not exhibiting an overt phenotype and failing to phenocopy
283 morphants have been previously reported[22–24]. El-Brolosy et al. proposed transcriptional
284 adaptation triggered by mutant RNA degradation as a mechanism to explain this discrepancy[15,25].
285 According to this model, decay of the mutant mRNA results in upregulation of related genes,
286 alleviating or suppressing the phenotype observed in morphants. Although a slight increase in
287 *desmb* mRNA expression was observed in *desma*^{kg97} embryos, no *desmb* mRNA upregulation and
288 Desmin protein expression have been detected in *desma*^{kg97} adult skeletal muscle, suggesting that
289 the compensating gene in fish carrying our *desma* allele is not *desmb*, the only gene known to have
290 high and extensive homology to *desma*. However, we found that vimentin mRNA level was
291 upregulated by approximately 10-fold in *desmb*^{kg156} adult skeletal muscles (Supplementary Fig. S4
292 online). Vimentin and desmin are closely related members of the class III intermediate filament
293 (IF) proteins, vimentin being the major IF protein expressed early in development and in
294 mesenchymal cells while desmin remains as the main IF protein expressed in muscle[26]. In zebrafish
295 embryos, vimentin expression is restricted to the developing brain and in adult tissues, vimentin

296 mRNA and protein are only detected in skin and eye[27]. The mechanisms underlying vimentin
297 upregulation in *desmb*^{kg156} mutants need further investigation. Genetic adaptation by yet unknown
298 adapting genes could explain the milder phenotype observed in mutants created in our study
299 compared to desmin morphants. However, it has been shown that *desma*^{sa5} allele results in a
300 muscle phenotype similar to that of morphants, even though the *desma*^{sa5} allele predicts an in-
301 frame stop codon and no *desma* mRNA was detected in mutants[14,21]. The specific mechanism
302 leading to the absence of mRNA was not investigated either in *desma*^{sa5} mutants or in the present
303 study. It is possible that the *desma*^{sa5} allele is not as efficient as *desma*^{kg97} allele in triggering an
304 adaptation mechanism for yet unknown reasons. It will be interesting to compare these models in
305 the contexts of mRNA decay and transcriptional adaptation. Alternatively, short truncated
306 polypeptides not detected in Western blot might play a role in this process before being rapidly
307 degraded. In conclusion, unraveling modifier genes and proteins that compensate for the loss of
308 desmin in our models will bring further insights in the role of desmin in muscle.

309 We found that the amplitude of calcium signals released in response to a depolarizing
310 current stimulus was significantly lower accompanied by a faster decay in *desma*^{kg97} skeletal
311 muscle fibres compared to WT. In desmin-null mice, it was shown that the lack of desmin
312 significantly altered the decay rate of the Ca^{2+} transient and depressed the speed of Ca^{2+} uptake
313 into the sarcoplasmic reticulum which caused a rise in cytosolic Ca^{2+} concentration at rest[28].
314 Similarly, knockdown of desmin in rat cardiomyocytes decreased the Ca^{2+} concentration in the
315 sarcoplasmic reticulum and has been related to inhibition of SERCA2 expression[29]. Impaired
316 mitochondrial morphology, positioning and respiratory function have been reported in human and
317 mice skeletal and cardiac muscles harboring various desmin mutations. Disruption of the inner
318 mitochondrial membrane and cristae organization has been observed in desmin-deficient mice
319 cardiomyocytes[30]. The contribution of mitochondrial calcium uptake in regulating calcium
320 homeostasis in skeletal muscle cells remains poorly understood; however, several studies have
321 linked the dysregulation of mitochondrial calcium uptake to altered skeletal muscle function[31,32].
322 Particularly, it was shown that aggregate-prone mutations in mice desmin gene cause a reduction
323 in the capacity of mitochondrial calcium uptake upon both electrical and chemical stimulation of
324 myotubes[33]. In zebrafish, disruption of mitochondrial cristae organization has been observed in
325 skeletal muscle of an aggregation prone *desma*-knockin line while *desma*^{sa5} knockout mutants
326 presented with normal mitochondria; however, defects in heart calcium flux were observed in both

327 mutants and linked to mislocalization of ryanodine receptors[14]. Similarly, in our study,
328 mitochondrial shape and structure was not affected in *desma*^{kg97} adult skeletal muscle tissue while
329 calcium flux was altered. Further investigation is needed to gain insight into the mechanism
330 underlying defective calcium signaling in desmin-null zebrafish mutants.

331 # METHODS

332 **Ethical approval and zebrafish maintenance**

333 All animal procedures were performed in accordance with Turkish *Animal Protection Act* 2004
334 and later modifications conforming to all relevant guidelines and regulations, and approved by the
335 Hacettepe University Animal Experimentations Local Ethics Board (Approval no. 2014/07-08).
336 The work in the UK was performed under UK Home Office license in accordance with the UK
337 *Animal (Scientific Procedures) Act 1986* and subsequent modifications. Adult zebrafish (AB)
338 (*Danio rerio*) were kept in 14/10 hr light-dark cycle at 28.5ºC. Adults are fed twice a day, with
339 dry feed in morning and *Artemia spp.* in evening. For spawning, male and female fish were placed
340 in a breeding tank with a separator. Next morning the separator was removed, viable eggs were
341 collected and rinsed in E3 medium (5 mM NaCl, 0.17 mM KCl, 0.33 mM $CaCl_2$, 0.33 mM $MgSO_4$,
342 10^{-5}% Methylene Blue). Embryos were kept in E3 medium for five days and placed into adult
343 tanks containing system water. Embryos were fed five times a day with dry feed and Artemia.

344 **Whole mount *in situ* hybridization**

345 Embryos were fixed in 4% PFA in PBS (w/v) overnight at 4°C, dehydrated in 50% and %100
346 methanol washes and stored at -20°C at least overnight before use. Probe templates were amplified
347 from cDNA isolated from 96 hpf wild-type embryos. Reverse primers for antisense probe
348 contained T3 promoter sequence while forward primers for sense probes contained T7 promoter
349 sequence. Primers sequences can be found as Supplementary Table S1 online. Digoxigenin-
350 labelled probes were generated using T3 or T7 RNA polymerases. Whole mount *in situ* mRNA
351 hybridization was performed as described[34]. Embryos were photographed as on Zeiss Axiophot
352 with Axiocam (Carl Zeiss, Oberkochen, Germany) using Openlab software (Agilent, Santa Clara,
353 CA, USA).

354

355 **Generation of mutant zebrafish lines**

356 CRISPR-Cas9 genome editing was performed as described in Fin et al[24]. CRISPR-Cas9 sgRNAs
357 showing minimal off-target sites were designed by using the online software ZiFiT Targeter.
358 Oligos encoding sgRNAs targeting the first exon of *desma* (GRCz11, Chr9: 7539113-7539132,
359 GGTCACCTCGTAAACTCTGG) and *desmb* (GRCz11, Chr6: 13891417-13891437,
360 GGCTATACTCGCTCTTATGG) were cloned into pDR274 plasmid (Addgene). sgRNAs were
361 synthesized using T7 RiboMAX Large Scale RNA production system (Promega) following the
362 manufacturer's protocol. Transcribed sgRNAs were purified using sodium acetate and ethanol
363 precipitation and quantified on Qubit fluorometer. Cas9 mRNA was transcribed from pCS2-Cas9
364 plasmid using mMessage mMachine SP6 Kit (Ambion) and purified by lithium chloride
365 precipitation. One-cell stage embryos were injected with 2 nl containing 80-200 pg of sgRNA and
366 100 pg of Cas9 mRNA. At 48 hpf, ten embryos were analysed for mosaicism at targeted loci using
367 high resolution melt analysis. Injected embryos were raised to adulthood and back-crossed to
368 identify transmitted mutations in F1 progeny. Homozygotes for each gene were generated by in-
369 cross of F2 heterozygotes. Primers sequences used for genotyping by Sanger sequencing can be
370 found as Supplementary Table S1 online.

371 **Quantitative real-time PCR**

372 Total RNA was isolated from a pool of 20 mechanically homogenized embryos at 96 hpf for each
373 sample (n=4) using TRItidy G (AppliChem) and 500 ng of cDNA was synthesized using
374 QuantiTect Reverse Transcription Kit (Qiagen) according to manufacturer's protocol. Primer
375 sequences for *desma* (covering both *desma-1* and *desma-2*), *desmb* and *actb1* can be found as
376 Supplementary Table S1 online. qPCR was performed in triplicates using SensiFAST SYBR No-
377 ROX Kit (Bioline) in Rotor-Gene 6000 (Corbett Life Science). *Desma* and *desmb* expression
378 levels were normalized to *actb1* expression, mutant expression levels were calculated relative to
379 wild-type using ΔΔCt method[35].

380 **Protein Extraction and Immunoblotting**

381 For protein extraction, 1-year-old fish were euthanized using overdose of tricaine (MS222, 300
382 mg/l). Skeletal muscle tissue was immediately dissected and fresh-frozen in liquid nitrogen. Tissue
383 was pulverized and homogenized in blending buffer (16 M Tris HCl, 200 M EDTA, 20% SDS,

384 1X protease inhibitor cocktail, volume adjusted to 5 ml with dH_2O) by sonication on ice. Lysates
385 were then centrifuged and supernatant transferred in a fresh tube. Total protein concentrations were
386 determined by bicinchoninic acid Protein Assay (Pierce, 23225). Equal amounts of protein (40 µg)
387 were loaded on a 13% polyacrylamide gel and transferred onto a nitrocellulose membrane using
388 semi-dry transfer, blocked for one hour at room temperature (%5 nonfat dried milk in %0,2 TBS-
389 T) and probed with anti-desmin antibody (1:1000; Sigma-Aldrich, D8281) overnight at 4°C or
390 anti-lamin B1 antibody (Abcam, ab90169) followed by appropriate HRP-conjugated secondary
391 antibody. Chemiluminescence detection was done by using SuperSignal™ West Femto Maximum
392 Sensitivity substrate (Thermo Scientific, 34095) in GeneGnome device. See Supplementary Fig.
393 S5 for uncropped full-length pictures of western blotting membranes.

394 **Whole-mount Immunofluorescence**

395 96 hpf embryos were fixed in %4 PFA overnight at +4°C and washed with PBTx (%0.01 Triton
396 X-100 in PBS). Embryos were permeabilized in 50 µg/ml Proteinase K for 2 hours and re-fixed in
397 2% PFA for 20 minutes at room temperature. Embryos were blocked in %5 BSA for 2 h at room
398 temperature and incubated with anti-desmin antibody (1:20; Sigma, D8281) for two overnights.
399 After two overnight incubations with Alexa-Fluor 488 conjugated secondary antibody, embryos
400 were mounted with DAPI onto glass bottom dishes for imaging with Zeiss LSM Pascal laser
401 scanning confocal microscope.

402 **Larval Phenotype and Morphology**

403 After successful mating, embryos were collected, counted and recorded for the following rates.
404 Hatching rate was reported as cumulative percentage of hatched embryos at 24 hpf, 48 hpf and 72
405 hpf. Mortality rate was expressed as the percentage of death embryos for 5 dpf. For body length
406 measurements, at least 16 embryos at 96 hpf were mounted, photographed (The Imaging Source,
407 DFK 41AU02) and measured from the mouth tip to the tail base using ImageJ (Version 1.49u).
408 Values for body length were presented as mean body length in cm. All the experiments except
409 body length measurements (three times) were performed at least eight times.

410 **Phalloidin Staining**

411 Phalloidin staining was performed on 96 hpf embryos (N=8) as described[36]. Following fixation in
412 4% PFA and permeabilization with 50 µg/ml Proteinase K, embryos were incubated in Alexa-

413 Fluor 488 conjugated Phalloidin (Invitrogen, A12379) overnight at +4ºC. Embryos were then
414 mounted onto glass bottom dishes and photographed with Zeiss LSM Pascal laser scanning
415 confocal microscope. Somite lengths were measured by using ImageJ (Version 1.49u).

416 **Hematoxylin Eosin Staining**

417 Adult zebrafish were freshly frozen in methyl-butanol cooled down in liquid nitrogen and then
418 taken into O.C.T compound for sectioning. 8 µm-thick tissue sections were incubated in
419 hematoxylin for 5 minutes, 1% acid-alcohol solution for 1 minute, 1% ammonia for 1 minute,
420 eosin solution for 3 minutes respectively by washing with distilled water in between steps. Finally,
421 sections were washed with alcohol and xylene, and mounted. Sections were examined under Nikon
422 Eclipse E-400 microscope and photographed by DXM 1200F digital camera.

423 **Transmission Electron Microscopy**

424 Fixation was performed by immersion in 2% glutaraldehyde in PBS for 3 hours, and the post
425 fixation by 1% osmium tetroxide in the dark for 1 hour at room temperature. Fixed tissues were
426 dehydrated in graded ethanol series, cleared in propylene oxide and embedded in epon (Agar
427 Scientific, UK). Forty two-sixty nanometer thick ultrathin sections were stained with uranyl
428 acetate and lead citrate, analyzed under a transmission electron microscope (JEOL-JEM 1400,
429 Japan) and attached CCD camera (Gatan Inc., Pleasanton, CA, USA)[37]. Striated muscle
430 ultrastructure has been evaluated for sarcolemma, myofibrils and cytoskeleton, nucleus,
431 mitochondria, membrane systems, deposits and particles and other unusual structures[38].

432 **Motility Assay**

433 For motility assay 48 hpf embryos from in-crosses of *desma*$^{kg97/+}$, *desmb*$^{kg156/+}$ or
434 *desma*$^{kg97/+}$;*desmb*$^{kg156/kg156}$ adults were used. Motility assays were performed by previously
435 described protocol[18]. A petri dish was placed on a transparent sheet with concentric circles 5 mm
436 apart. One embryo at a time was positioned in the center of the dish and stimulated using a
437 dissection needle. The escape response of the embryo was recorded using a high-speed camera
438 (Huawei, Mate 10 Lite, 16 MP, 120 fps). The movements of the embryo—midpoint between the
439 two eyes—were tracked using a custom software that works based on template matching
440 algorithm. The elapsed time between the last frame before touch stimulus and the first frame after
441 the body of the fish contacts the 10 mm circle was computed from the digitized embryo movements

442 with a resolution of 8.3 ms (120 fps). Experiments were performed blindly and after video
443 accusation, DNA was extracted from each embryo for genotyping.

444 **Calcium Flux**

445 1-year-old fish were euthanized using overdose of tricaine (MS222, 300 mg/l). After removal of
446 the skin, tissue samples were incubated into 5 mg/ml collagenase solution in PBS (without Ca^{2+}
447 and Mg^{2+}) at 28.5 °C for 20 minutes on a shaker at 50 rpm. Samples have been triturated gently
448 under dissecting microscope in order to dissociate muscle fibres from the tissue components until
449 rode-shaped muscle fibres were obtained. Dissociated fibres were incubated in DMEM containing
450 10% FBS and 1% antibiotic-antimycotic overnight at 28.5 °C and 5% CO_2 environment. On the
451 following day, fibres were incubated in 2.5 µM Fluo-4 AM for 20 minutes in 5% CO_2. Under a
452 laser scanning confocal microscope (Zeiss LSM Pascal), glass microelectrodes (filled with 3M
453 KCl) were inserted into muscle fibres in a current clamp mode[39]. A depolarizing current stimulus
454 was delivered through the microelectrode to excite the fibre and evoke a calcium signal. The
455 evoked calcium-specific fluorescent emission signal was recorded in "Line Scan" mode of
456 confocal microscope, supplying information about a line cross sectioning the muscle fibre at a high
457 frequency in tandem with the electrical recordings. Data were analyzed in MATLAB (The
458 MathWorks, Inc). The stimulus waveform, which consisted of four consecutive pulses increasing
459 in duration, was used in all the experiments. The amplitude of the current pulse was kept constant
460 at 100 nA while the durations were 10 ms, 20 ms, 30 ms, 40 ms respectively. Experiments were
461 done by using three WT, three *desma*$^{kg97/kg97}$ and two *desmb*$^{kg156/kg156}$ fish and at least eight fibres
462 from each group were recorded.

463 ## Statistics

464 Data were statistically analyzed by GraphPad Prism 8 (GraphPad Software Inc.) by nonparametric
465 Mann-Whitney U test (Two-tailed) when two groups were compared. The results were considered
466 significant when $P<0.05$. For analysis of time course experiments (hatching rate, mortality rate
467 and time course calcium flux), repeated measures two-way ANOVA was used and Bonferroni post
468 *hoc* test was used for multiple comparisons. All error bars were presented as mean±SEM and bars
469 were represented as median.

470

Acknowledgements

This work was supported by The Scientific and Technological Research Council of Turkey, Project no. 214S174 to P.R.D. S.M.H. is an MRC Scientist with MRC Programme Grant G1001029 and MR/N021231/1 support.

Competing interests

The author(s) declare no competing interests.

Data Availability

Supporting information is available in Supplementary files online and further information is available from the corresponding author upon request.

References

1. Clemen, C. S., Herrmann, H., Strelkov, S. V. & Schröder, R. Desminopathies: Pathology and mechanisms. *Acta Neuropathol.* **125**, 47-45 (2013).
2. Dagvadorj, A. *et al.* Respiratory insufficiency in desminopathy patients caused by introduction of proline residues in desmin C-terminal α-helical segment. *Muscle Nerve* **27**, 669-75(2003).
3. Ariza, A. *et al.* Desmin myopathy: a multisystem disorder involving skeletal, cardiac, and smooth muscle. *Hum. Pathol.* **26**, 1032-7 (1995).
4. Goldfarb, L. G. *et al.* Missense mutations in desmin associated with familial cardiac and skeletal myopathy. *Nat. Genet.* **19**, 402-3 (1998).
5. Cetin, N. *et al.* A novel desmin mutation leading to autosomal recessive limb-girdle muscular dystrophy: distinct histopathological outcomes compared with desminopathies. *J. Med. Genet.* **50**, 437–43 (2013).
6. Bär, H. *et al.* Conspicuous involvement of desmin tail mutations in diverse cardiac and skeletal myopathies. *Hum. Mutat.* **28**, 374-86 (2007).
7. Li, Z. *et al.* Cardiovascular lesions and skeletal myopathy in mice lacking desmin. *Dev. Biol.* **175**, 362-6 (1996).
8. Milner, D. J., Weitzer, G., Tran, D., Bradley, A. & Capetanaki, Y. Disruption of muscle architecture and myocardial degeneration in mice lacking desmin. *J. Cell Biol.* **134**, 1255-70 (1996).

500 9. Lin, Y. Y. Muscle diseases in the zebrafish. *Neuromuscul. Disord.* **22**, 673-84 (2012).
501 10. Berger, J. & Currie, P. D. Zebrafish models flex their muscles to shed light on muscular
502 dystrophies. *Dis. Model. Mech.* **5**, 726–32 (2012).
503 11. Gibbs, E. M., Horstick, E. J. & Dowling, J. J. Swimming into prominence: the zebrafish as
504 a valuable tool for studying human myopathies and muscular dystrophies. *FEBS J.* **280**,
505 4187–97 (2013).
506 12. Vogel, B. *et al.* In-vivo characterization of human dilated cardiomyopathy genes in
507 zebrafish. *Biochem. Biophys. Res. Commun.* **390**, 516–522 (2009).
508 13. Li, M., Andersson-Lendahl, M., Sejersen, T. & Arner, A. Knockdown of desmin in
509 zebrafish larvae affects interfilament spacing and mechanical properties of skeletal
510 muscle. *J. Gen. Physiol.* **141**, 335–345 (2013).
511 14. Ramspacher, C. *et al.* Developmental Alterations in Heart Biomechanics and Skeletal
512 Muscle Function in Desmin Mutants Suggest an Early Pathological Root for
513 Desminopathies. *Cell Rep.* **11**, 1564–76 (2015).
514 15. El-Brolosy, M. A. *et al.* Genetic compensation triggered by mutant mRNA degradation.
515 *Nature* **568**, 193–197 (2019).
516 16. Kimmel, C. B., Ballard, W. W., Kimmel, S. R., Ullmann, B. & Schilling, T. F. Stages of
517 Embryonic Development of the Zebrafish. *Dev. Dyn.* **203**, 253–310 (1995).
518 17. Skobo, T. *et al.* Zebrafish ambra1a and ambra1b knockdown impairs skeletal muscle
519 development. *PLoS One* **9**, e99210 (2014).
520 18. Goody, M. F. *et al.* NAD+ Biosynthesis Ameliorates a Zebrafish Model of Muscular
521 Dystrophy. *PLoS Biol.* **10**, e1001409 (2012).
522 19. Campbell, J. M., Hartjes, K. a, Nelson, T. J., Xu, X. & Ekker, S. C. New and TALENted
523 genome engineering toolbox. *Circ. Res.* **113**, 571–87 (2013).
524 20. Hnia, K., Ramspacher, C., Vermot, J. & Laporte, J. Desmin in muscle and associated
525 diseases: beyond the structural function. *Cell Tissue Res.* **360**, 591-608 (2015).
526 21. Ramspacher, C. *et al.* Developmental Alterations in Heart Biomechanics and Skeletal
527 Muscle Function in Desmin Mutants Suggest an Early Pathological Root for
528 Desminopathies. *Cell Rep.* **11**, 1564–1576 (2015).
529 22. Kok, F. O. *et al.* Reverse genetic screening reveals poor correlation between morpholino-
530 induced and mutant phenotypes in zebrafish. *Dev. Cell* **32**, 97-108 (2015).

531 23. Law, S. H. W. & Sargent, T. D. The serine-threonine protein kinase PAK4 is dispensable
532 in zebrafish: Identification of a morpholino-generated pseudophenotype. *PLoS One* **9**,
533 e100268 (2014).
534 24. Fin, L., Bergamin, G., Steiner, R. A. & Hughes, S. M. The Cannabinoid Receptor
535 Interacting Proteins 1 of zebrafish are not required for morphological development,
536 viability or fertility. *Sci. Rep.* **7**, 1–9 (2017).
537 25. Rossi, A. *et al.* Genetic compensation induced by deleterious mutations but not gene
538 knockdowns. *Nature* **524**, 230–233 (2015).
539 26. Tokuyasu, K. T., Maher, P. A. & Singer, S. J. Distributions of vimentin and desmin in
540 developing chick myotubes in vivo. II. immunoelectron microscopic study. *J. Cell Biol.*
541 **100**, 1157-1166 (1985).
542 27. Cerdà, J., Conrad, M., Markl, J., Brand, M. & Herrmann, H. Zebrafish vimentin:
543 Molecular characterisation, assembly properties and developmental expression. *Eur. J.*
544 *Cell Biol.* **77**, 175–187 (1998).
545 28. Goodall, M. H., Ward, C. W., Pratt, S. J. P., Bloch, R. J. & Lovering, R. M. Structural and
546 functional evaluation of branched myofibers lacking intermediate filaments. *Am. J.*
547 *Physiol. Physiol.* **303**, C224–C232 (2012).
548 29. Chen, L. *et al.* The role of desmin alterations in mechanical electrical feedback in heart
549 failure. *Life Sci.* **241**, 117-119 (2020).
550 30. Diokmetzidou, A. *et al.* Desmin and αB-crystallin interplay in the maintenance of
551 mitochondrial homeostasis and cardiomyocyte survival. *J. Cell Sci.* **129**, 3705–3720
552 (2016).
553 31. Debattisti, V. *et al.* Dysregulation of Mitochondrial Ca2+ Uptake and Sarcolemma Repair
554 Underlie Muscle Weakness and Wasting in Patients and Mice Lacking MICU1. *Cell Rep.*
555 **29**, 1274-1286.e6 (2019).
556 32. Díaz-Vegas, A. R. *et al.* Mitochondrial Calcium Increase Induced by RyR1 and IP3R
557 Channel Activation After Membrane Depolarization Regulates Skeletal Muscle
558 Metabolism. *Front. Physiol.* **9**, 791 (2018).
559 33. Smolina, N., Bruton, J., Sjoberg, G., Kostareva, A. & Sejersen, T. Aggregate-prone
560 desmin mutations impair mitochondrial calcium uptake in primary myotubes. *Cell*
561 *Calcium* **56**, 269–275 (2014).

562 34. Hinits, Y. & Hughes, S. M. Mef2s are required for thick filament formation in nascent
563 muscle fibres. *Development* **134**, 2511-9 (2007).
564 35. Schmittgen, T. D. & Livak, K. J. Analyzing real-time PCR data by the comparative CT
565 method. *Nat. Protoc.* **3**, 1101-8 (2008).
566 36. Goody, M. & Henry, C. Phalloidin staining and immunohistochemistry of embryos.
567 http://www.bio-protocol.org/e786, *Bio-Protocol* **3** (2013).
568 37. Yersal, N. *et al.* Leptin promotes proliferation of neonatal mouse stem/progenitor
569 spermatogonia. *J. Assist. Reprod. Genet.* **37**, 2825–2838 (2020).
570 38. Dubowitz, V., Sewry, C. & Oldfors, A. 5- Ultrastructural Changes' in *Muscle Biopsy - 5th*
571 *Edition* (Elsevier, 2020).
572 39. Purali, N. Fast calcium transients translate the distribution and conduction of neural
573 activity in different regions of a single sensory neuron. *Invertebr. Neurosci.* **17**, 7 (2017).

574 ## Author Contributions

575 P.R.D. designed, P.R.D. and S.M.H. supervised the study. G.K.K. wrote the paper and assembled
576 the figures, E.K.M. made contribution to writing the paper. G.K.K., E.K.M, C.K., S.U., B.S., B.E.,
577 M.G., I.U., N.B.D., P.K., B.T. and N.P. performed the experiments and/or analyzed the results.
578 All authors interpreted the data and edited the manuscript.

579 ## Figure Legends

580 **Fig. 1. Whole mount *in situ* mRNA hybridisation of embryos at the indicated stages for**
581 **antisense probes to *desma* and *desmb*.** (**a**) Lateral views are anterior to top, dorsal to left for 13-
582 22 hpf; anterior to left except 11 hpf which is a dorsal view. 48-120 hpf whole mounts are anterior
583 to left, dorsal to top. Scale bar: 250 µm. (**b**) Arrows indicate heart in frontal view for left panel
584 (*desma*) and ventral view for right panel (*desmb*) of 35 hpf embryos. (**c**) Transversal sections where
585 dorsal is top. (**d**) Upper left panel is a lateral view at 96 hpf, scale bar: 250 µm. Dashed line
586 represents the position of the transversal section in upper right panel where dorsal is top, scale bar:
587 100 µm. Lower panels are lateral views of zebrafish heads at 72 and 120 hpf treated with *desma*
588 probe. Scale bar: 100 µm. (**e**) Left panel is a ventral view with anterior at top. Right panels are
589 lateral views. Ai, anterior intestine; eom, extraocular muscles; fast, fast muscles; fm, pectoral fin
590 muscles; hm, hypaxial muscles; mdm, mandibular muscles; om, opercular muscles; slow, slow
591 muscles; som, somites. Scale bar: 250 µm.

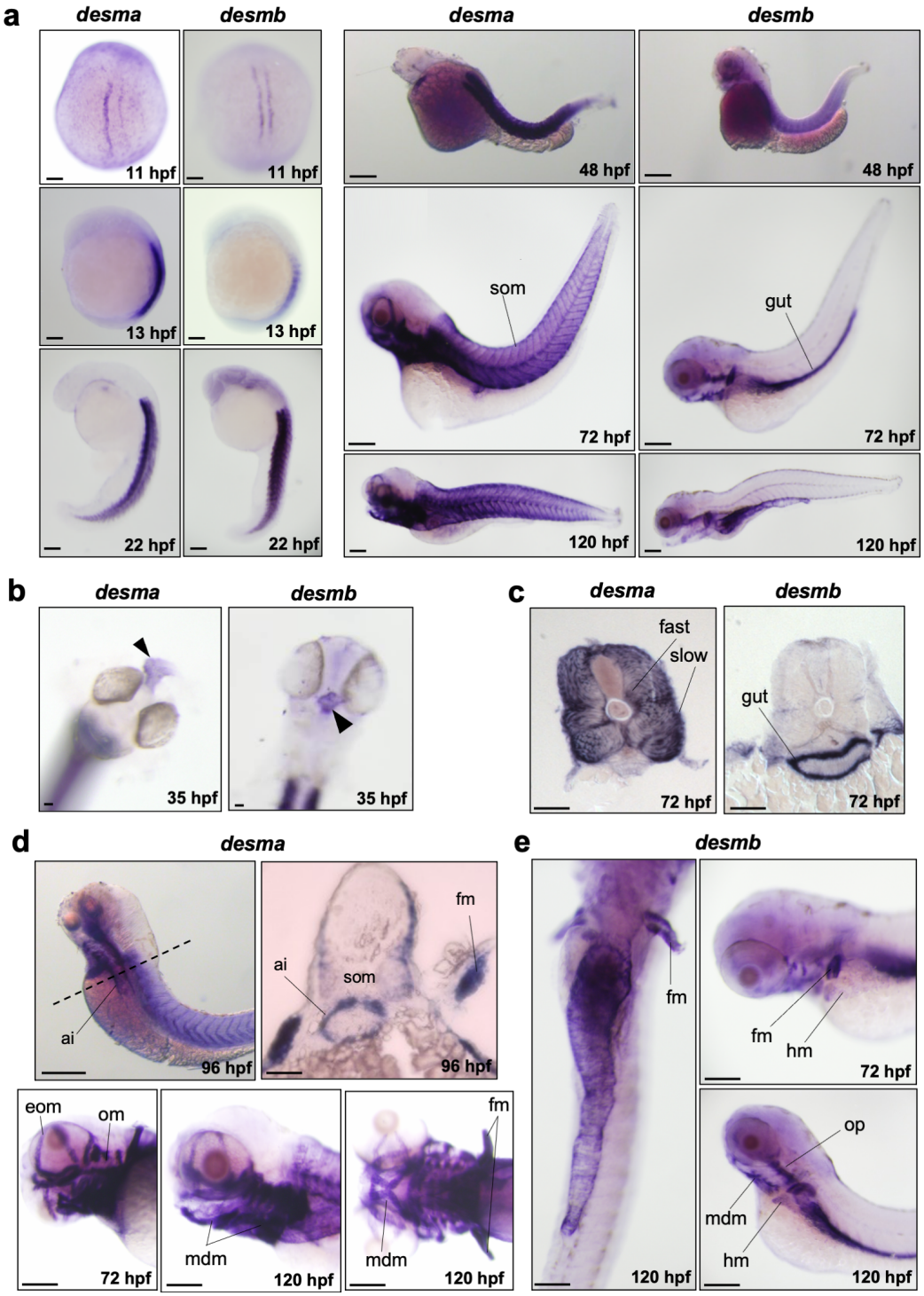
a
desma
desmb
desma
desmb
11 hpf
11 hpf
48 hpf
48 hpf
13 hpf
13 hpf
som
gut
72 hpf
72 hpf
22 hpf
22 hpf
120 hpf
120 hpf
b
desma
desmb
35 hpf
35 hpf
c
desma
desmb
fast
slow
gut
72 hpf
72 hpf
d
desma
ai
96 hpf
fm
ai
som
96 hpf
eom
om
72 hpf
mdm
120 hpf
fm
mdm
120 hpf
e
desmb
fm
120 hpf
fm
hm
72 hpf
op
mdm
hm
120 hpf

592

593

594 **Fig. 2. Generation of *desma* and *desmb* knockout lines. (a)** Alignments and chromatograms of
595 wild-type DNA sequences with mutant alleles, and predicted mutant polypeptide sequences. In
596 DNA sequences, yellow highlights gRNA target sequence, hyphens show deleted bases, inserted
597 bases are indicated in red font. In protein sequences, the first residue affected by the frameshift is
598 indicated in red font, asterisks represent early stop codons. (**b**) Quantitative real-time PCR results
599 showing the expression of *desma* and *desmb* mRNA in wild-type and homozygous mutant 96 hpf
600 embryos (N=4, Mann-Whitney U). (**c**) Left panel shows whole mount *in situ* mRNA hybridisation
601 of $desma^{kg97}$ homozygous embryos at the indicated stages for antisense probes to *desmb*. Right
602 panel shows whole mount *in situ* mRNA hybridisation of $desmb^{kg156}$ homozygous embryos at the
603 indicated stages for antisense probes to *desma.* Scale bar: 250 µm. Ai, anterior intestine; som,
604 somite. (**d**) Brightfield pictures of 96 hpf WT and mutant embryos. Scale bar: 250 µm.

a

desma

WT CCTCAGGTTCCTCTGGCTCCTCAAGACTGACCTCCAGAGTTTACGAGGTGACCAAGAG

kg97 CCTCAGGTTCCTCTGGCTCCTCAAGACTGACCTCCA--TGATGTTTACGAGGTGACCA -2+4

Protein sequence

WT MSTKYSASAESASSYRRTFGSGLGSSIFAGHGSSGSSGSSRLTSRVYEVTKSSASPHF

kg97 MSTKYSASAESASSYRRTFGSGLGSSIFAGHGSSGSSGSSRLTSMMFTR*

desmb

WT CTCCTACAGCATGCCCAACTTGTCTGCAGGCTATACTCGCTCTTATGGTGGGATGGGT

kg156 CTCCTACAGCATGCCCAACTTGTCTGCAGGCTATACTCGCT-----GGTGGGATGGGT -5

Protein sequence

WT MSHSYATSSSSSYRRMFGGPGYMTP...PGFSGYRASSYSMPNLSAGYTRSYGGMGE

kg156 MSHSYATSSSSSYRRMFGGPGYMTP...PGFSGYRASSYSMPNLSAGYTRWWDG*

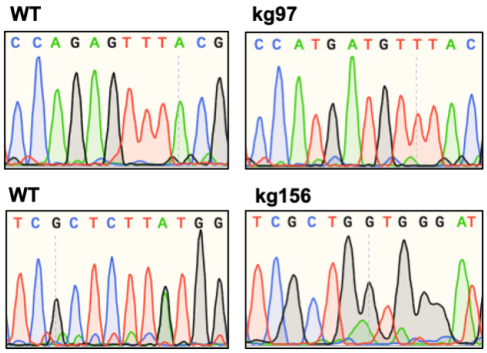

b

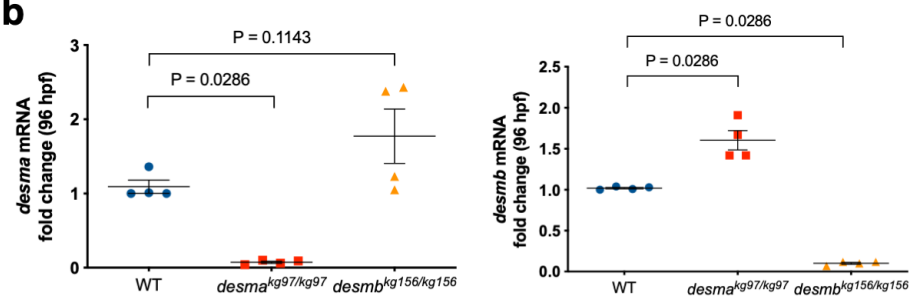

c

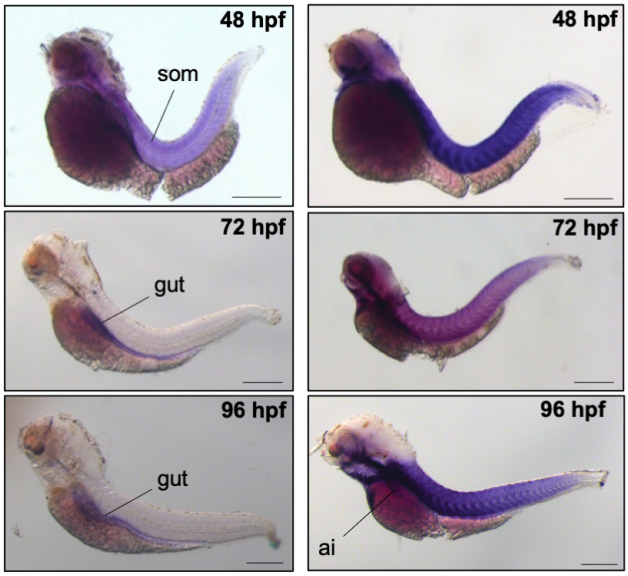

d

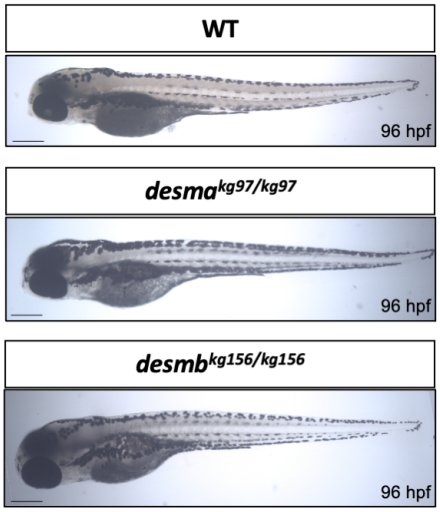

605

606

607

608

609

610

611 **Fig. 3. Desmin protein expression in 96 hpf embryos.** Whole mount immunofluorescence
612 staining of desmin with an anti-desmin polyclonal antibody (Sigma, D8281) recognizing both
613 Desma and Desmb, in wild-type and mutant 96 hpf embryos. Left upper panel is lateral view of a
614 WT embryo with anterior to left, dorsal to top, beneath is ventral view with anterior to left, white
615 arrowheads indicate the gut. Right upper panels are lateral views of *desma*$^{kg97/kg97}$ with anterior to
616 left, dorsal to top. Lower panel shows *desmb*$^{kg156/kg156}$ embryos with anterior to left, dorsal to top.
617 Scale bar: 500 µm. Boxes with dashed lines delineate areas that were zoomed and focused on
618 anterior and posterior segments of the intestine as shown in lower right panels, orange arrowheads
619 indicate anterior intestine, white arrowheads show middle and posterior segments of the intestine.

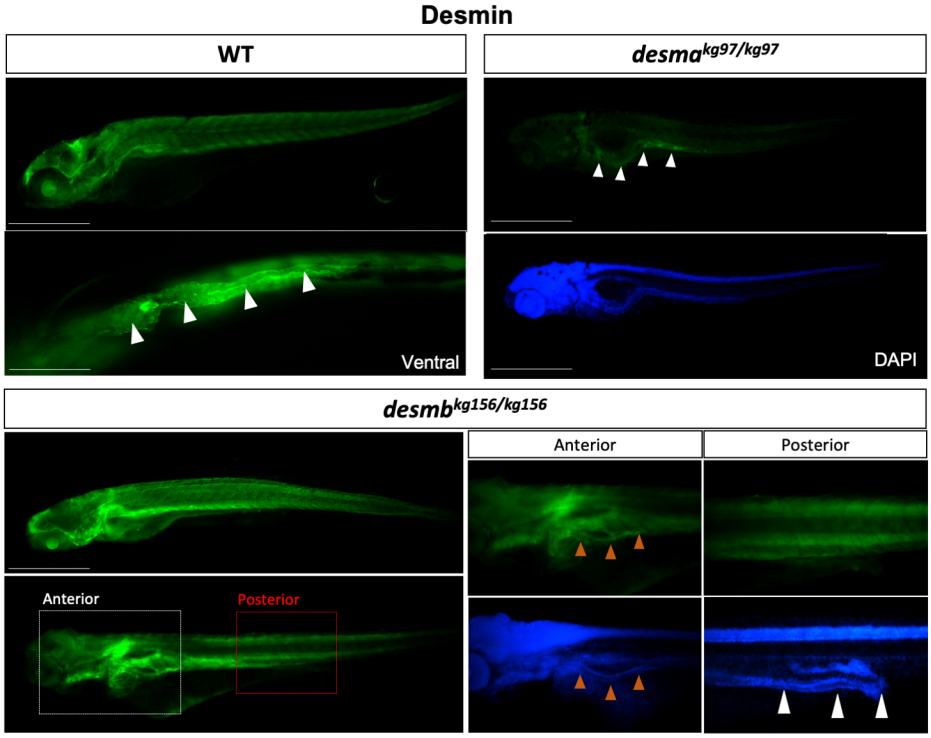

620

621 **Fig. 4. Evaluation of neuromuscular defect in mutant larvae.** (**a)** The number of viable embryos
622 after successful mating of WT fish (n=10) compared to homozygous *desma*^{kg97} (n=10) (*P*=0.6842,
623 Mann-Whitney U) or homozygous *desmb*^{kg156} (n=8) (*P*=0.9654, Mann-Whitney U) fish. (**b)**
624 Comparison of hatching rate between homozygous mutants and WT 24, 48 and 72 hpf embryos
625 At 72 hpf, no significant difference in the hatching rate was found between mutants and WT
626 (*desma*$^{kg97/kg97}$ vs. WT, *P*=0.9902; *desmb*$^{kg156/kg156}$ vs WT, *P*=0.3186, repeated measures two-way
627 ANOVA, Bonferroni post *hoc* test) (**c)** Body length of 96 hpf WT (N=18) and homozygous
628 *desma*^{kg97} (N=25) or homozygous *desmb*^{kg156} (N=16) mutant embryos (*P*=0.2036 for WT vs.
629 *desma*$^{kg97/kg97}$; *P*=0.1893 for WT vs. *desmb*$^{kg156/kg156}$, Mann-Whitney U). (**d)** Cumulative mortality
630 rate from 1 to 5 dpf homozygous *desma*^{kg97} mutants (N=1247) compared to WT (N=2460)
631 (*P*=0.1287, repeated measures two-way ANOVA, Bonferroni post *hoc* test) and homozygous
632 *desmb*^{kg156} mutants (N=2615) compared to WT (*P*=0.6239, repeated measures two-way ANOVA,
633 Bonferroni post *hoc* test). **(e)** Optical sections of the mid-trunk region of WT and homozygous
634 mutants 96 hpf embryos (N=8) stained with rhodamine phalloidin (F-actin) with insets showing
635 striations (asterisks indicate occasional wavy fibres in both WT and mutants). Scale bar: 50 µm.
636 (**f-h)** Touch-evoked escape time (ms) of 48 hpf embryos. Motility experiments were performed
637 blind on siblings from (**f**) *desma*$^{kg97/+}$, (**g**) *desmb*$^{kg156/+}$ or (**h**) *desma*$^{kg97/+}$*;desmb*$^{kg156/kg156}$ in-crosses
638 followed by *post hoc* genotyping. (**f**) Heterozygous *desma*^{kg97} embryos (N=23) were compared to
639 WT (N=9) (P=0.122, Mann-Whitney U) and *desma*$^{kg97/kg97}$ (N=15) compared to WT (P=0.5529,
640 Mann-Whitney U). (**g**) Heterozygous *desmb*^{kg156} embryos (N=6) were compared to WT (N=38)
641 (P=0.3968, Mann-Whitney U) and *desmb*$^{kg156/kg156}$ (N=6) compared to WT (P=0.6131, Mann-
642 Whitney U). (**h**) Homozygous double mutants (N=8) were compared to *desma*$^{+/+}$;*desmb*$^{kg156/kg156}$
643 (n=15) (*P*=0.3165, Mann-Whitney U) and *desma*$^{kg97/+}$*;desmb*$^{kg156/kg156}$ embryos (n=34) compared
644 to *desma*$^{+/+}$;*desmb*$^{kg156/kg156}$ (*P*=0.2334, Mann-Whitney U).

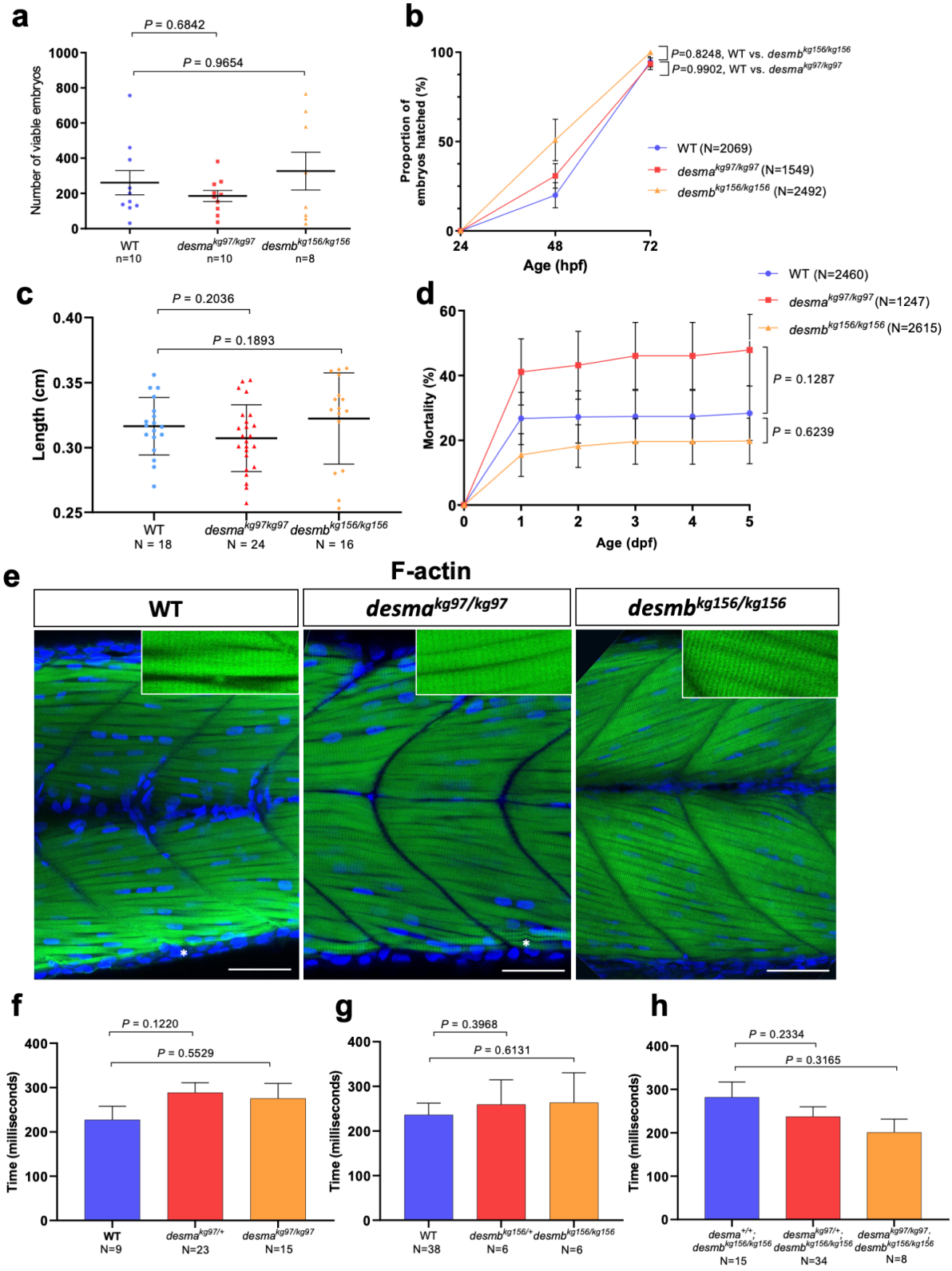
a
P = 0.6842
P = 0.9654
Number of viable embryos
1000
800
600
400
200
0
WT
n=10
desmakg97/kg97
n=10
desmbkg156/kg156
n=8
b
P=0.8248, WT vs. desmbkg156/kg156
P=0.9902, WT vs. desmakg97/kg97
Proportion of embryos hatched (%)
100
50
0
24
48
72
Age (hpf)
WT (N=2069)
desmakg97/kg97 (N=1549)
desmbkg156/kg156 (N=2492)
c
P = 0.2036
P = 0.1893
Length (cm)
0.40
0.35
0.30
0.25
WT
N = 18
desmakg97kg97
N = 24
desmbkg156/kg156
N = 16
d
WT (N=2460)
desmakg97/kg97 (N=1247)
desmbkg156/kg156 (N=2615)
Mortality (%)
60
40
20
0
P = 0.1287
P = 0.6239
0
1
2
3
4
5
Age (dpf)
e
F-actin
WT
desmakg97/kg97
desmbkg156/kg156
f
P = 0.1220
P = 0.5529
Time (milliseconds)
400
300
200
100
0
WT
N=9
desmakg97/+
N=23
desmakg97/kg97
N=15
g
P = 0.3968
P = 0.6131
Time (milliseconds)
400
300
200
100
0
WT
N=38
desmbkg156/+
N=6
desmbkg156/kg156
N=6
h
P = 0.2334
P = 0.3165
Time (milliseconds)
400
300
200
100
0
desma+/+; desmbkg156/kg156
N=15
desmakg97/+; desmbkg156/kg156
N=34
desmakg97/kg97; desmbkg156/kg156
N=8

645

Fig. 5. **Desmin protein expression and histological examination of adult skeletal muscle. (a)** Photographs of 1 yr-old anesthetized fish. (**b**) Immunoblotting of skeletal muscle protein extracts of WT, *desma*$^{kg97/kg97}$, *desma*$^{kg97/+}$, *desmb*$^{kg156/kg156}$, *desmb*$^{kg156/+}$ and *desma*$^{kg97/kg97}$;*desmb*$^{kg156/kg156}$ double mutant fish probed with anti-desmin antibody. Lamin B1 was labeled on the same blot as loading control. Uncropped full-length pictures of the blot is available in Supplementary Figure S5 online. (**c**) Transversal cryosections of mid-trunk somites from two different areas of WT and homozygous mutant adults stained with hematoxylin eosin showing no pathological changes. Scale bar: 25 µm.

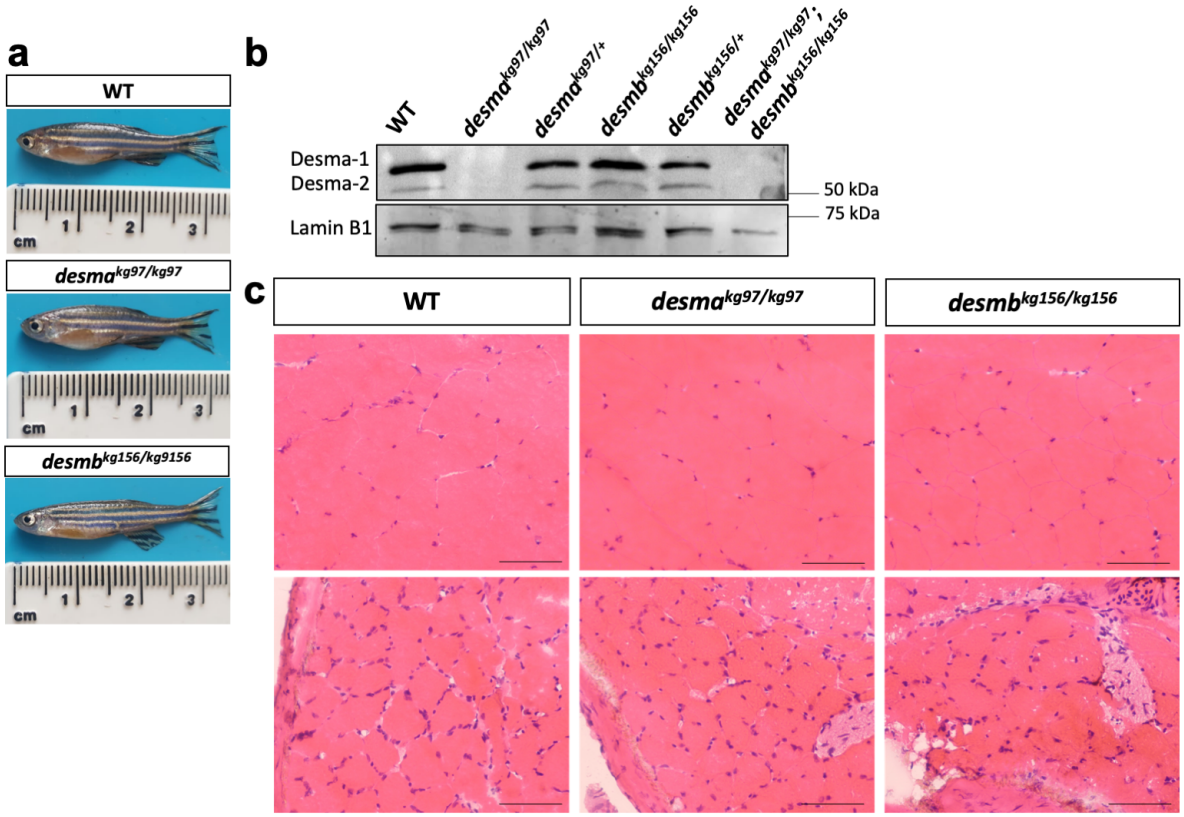

655 **Fig. 6. Ultrastructural features of adult WT and mutant skeletal muscle tissue.** First, second
656 and third columns present adult WT, *desma*$^{kg97/kg97}$, *desmb*$^{kg156/kg156}$ skeletal muscle tissues'
657 electron micrographs, respectively. First row indicates the generally aligned sarcomeric structures
658 with the presence of seldom disruptions (asterisks). Second row shows centrally (d) and
659 peripherally (e, f) located healthy nuclei (N) with peripherally condensed chromatin and well-
660 defined nucleoli. Third and fourth row (g-l) shows pleomorphic mitochondria (M) with well-
661 defined tubular cristae. Fifth and sixth rows present the Z line streaming (arrows in m-o) and
662 enlargement (m-r) of the T-tubule systems related to the triads (double arrows). Uranyl acetate,
663 lead citrate. HM, High Magnification. Magnifications are as follows: (a-c) 8000x, (d) 25000x, (e,f)
664 20000x, (g-i) 15000x, (j) 40000x, (k) 60000x, (l) 30000x, (m-o) 20000x, (p) 25000x and (q, r)
665 20000x.

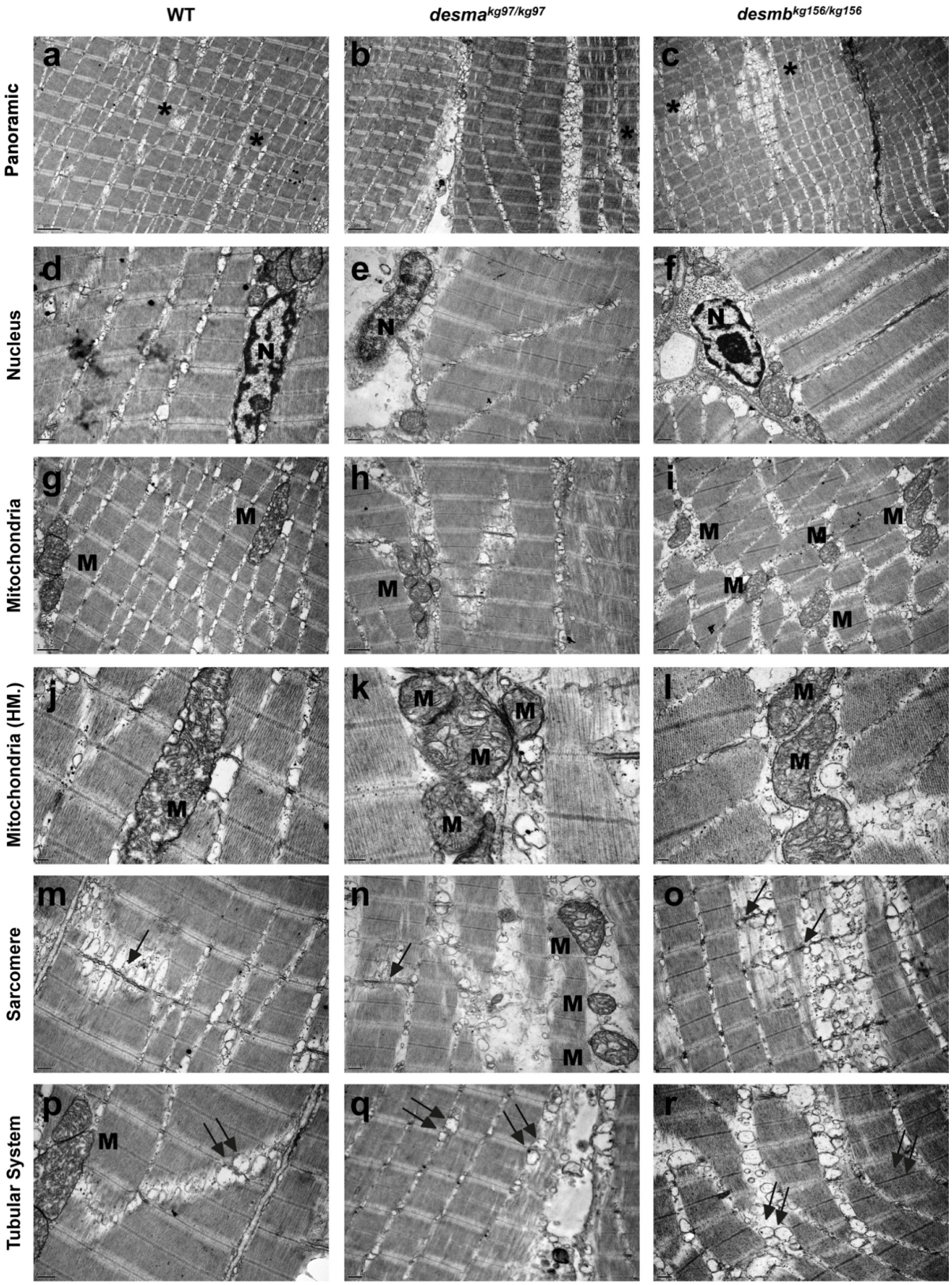
WT
desma kg97/kg97
desmb kg156/kg156
Panoramic
Nucleus
Mitochondria
Mitochondria (HM.)
Sarcomere
Tubular System
a
b
c
d
e
f
g
h
i
j
k
l
m
n
o
p
q
r
N
M

666

667 **Fig. 7. Calcium flux in isolated fibres.** (**a**) Calcium flux along fibres was monitored in vivo by
668 Fluo-4 AM after four consecutive depolarizing stimuli. Top panel, membrane potential responses
669 to current stimulus pulses with varying durations of 10, 20, 30, 40 ms with the amplitude of the
670 current pulse kept constant at 100 mV and the duration increased by 10 ms at each pulse. Middle
671 panel, evoked calcium transients in line scan mode (*tx*) to current stimuli. Bottom panel, integrated
672 emission signal as a function of time for each experimental group. (**b**) Membrane potential
673 response to the first stimulus of 10 ms (top) or to the fourth stimulus of 40 ms. (**c**) Baseline
674 corrected amplitude divided by fibre diameter (ΔF/μm) of the calcium emission signals during the
675 first (10 ms) stimulus and fourth (40 ms) stimulus were compared between mutants and WT. (**e**)
676 Time course analysis of the baseline corrected and normalized amplitude of the calcium transient
677 from the longest stimulus (40 ms) was represented as mean amplitude values as a function of time.
678 Homozygous $desma^{kg97}$ fibres (N=11, red curve) or homozygous $desmb^{kg156}$ fibres (N=8, orange
679 curve) were compared to WT (N=8, blue curve). (* indicates time points where $P<0.05$, repeated
680 measures two-way ANOVA, Bonferroni post *hoc* test).

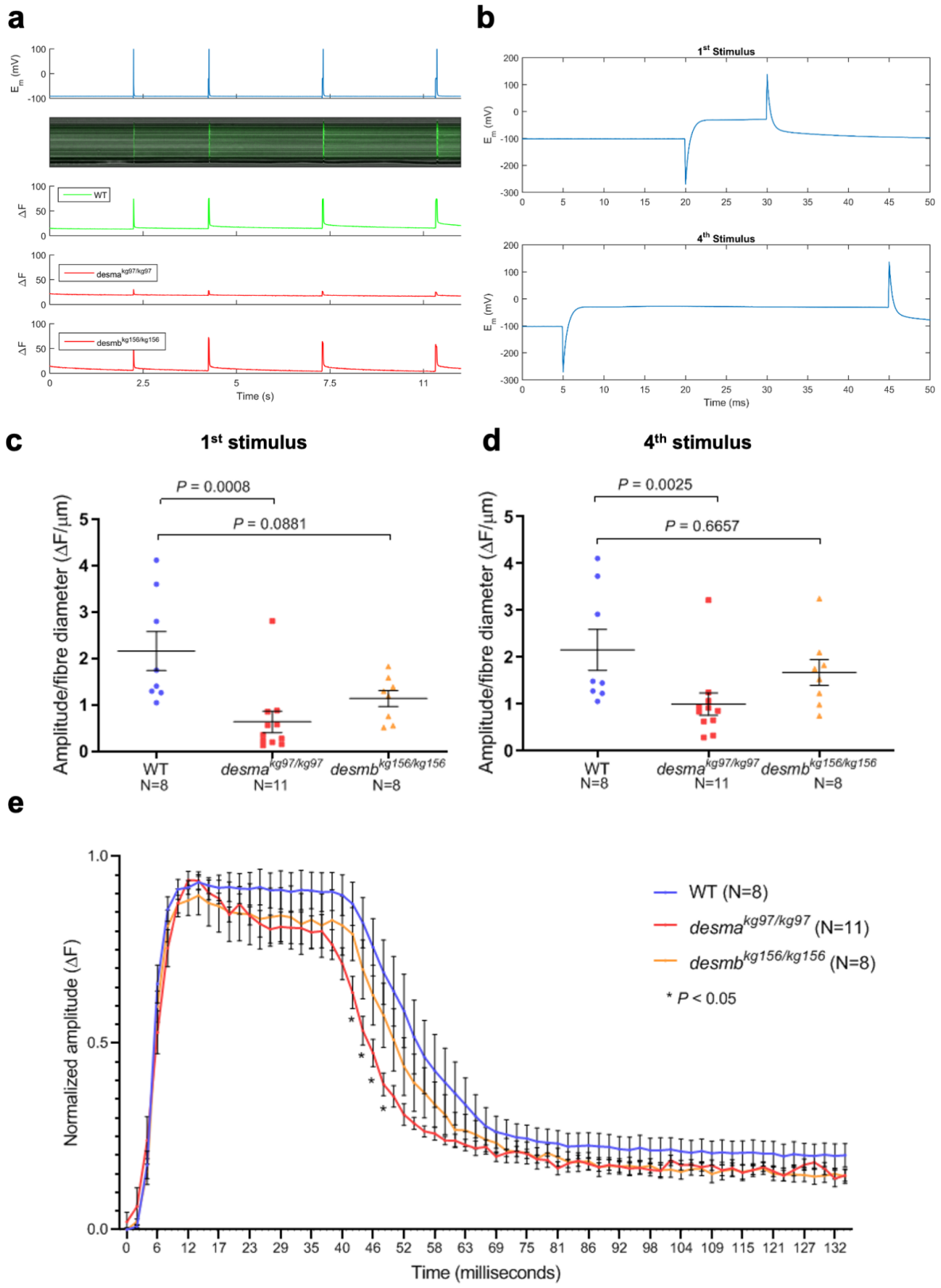
a
b
1st Stimulus
4th Stimulus
Time (s)
Time (ms)
WT
desma kg97/kg97
desmb kg156/kg156
c
1st stimulus
d
4th stimulus
P = 0.0008
P = 0.0881
P = 0.0025
P = 0.6657
Amplitude/fibre diameter (ΔF/μm)
WT N=8
desma kg97/kg97 N=11
desmb kg156/kg156 N=8
e
Normalized amplitude (ΔF)
Time (milliseconds)
WT (N=8)
desma kg97/kg97 (N=11)
desmb kg156/kg156 (N=8)
* P < 0.05

681